



Molecular Gas within the Milky Way's Nuclear Wind

Frances H. Cashman¹ , Andrew J. Fox² , Blair D. Savage³ , Bart P. Wakker³ , Dhanesh Krishnarao^{1,4,5} ,
Robert A. Benjamin⁶ , Philipp Richter⁷ , Trisha Ashley¹ , Edward B. Jenkins⁸ , Felix J. Lockman⁹ ,
Rongmon Bordoloi¹⁰ , and Tae-Sun Kim³

¹ Space Telescope Science Institute, 3700 San Martin Drive, Baltimore, MD 21218, USA; frcashman@stsci.edu

² AURA for ESA, Space Telescope Science Institute, 3700 San Martin Drive, Baltimore, MD 21218, USA; afax@stsci.edu

³ Department of Astronomy, University of Wisconsin-Madison, 475 North Charter Street, Madison, WI 53706, USA

⁴ NSF Astronomy & Astrophysics Postdoctoral Fellow, Johns Hopkins University, 3400 N. Charles Street, Baltimore, MD 21218, USA

⁵ Department of Physics, Colorado College, 14 East Cache La Poudre Street, Colorado Springs, CO 80903, USA

⁶ Department of Physics, University of Wisconsin-Whitewater, 800 West Main Street, Whitewater, WI 53190, USA

⁷ Institut für Physik und Astronomie, Universität Potsdam, Haus 28, Karl-Liebknecht-Str. 24/25, D-14476, Potsdam, Germany

⁸ Department of Astrophysical Sciences, Princeton University, Princeton, NJ 08544, USA

⁹ Green Bank Observatory, P.O. Box 2, Rt. 28/92, Green Bank, WV 24944, USA

¹⁰ Department of Physics, North Carolina State University, 421 Riddick Hall, Raleigh, NC 27695-8202, USA

Received 2021 November 10; revised 2021 November 21; accepted 2021 November 22; published 2021 December 9

Abstract

We report the first direct detection of molecular hydrogen associated with the Galactic nuclear wind. The Far-Ultraviolet Spectroscopic Explorer spectrum of LS 4825, a B1 Ib–II star at $l, b = 1.67^\circ, -6.63^\circ$ lying $d = 9.9_{-0.8}^{+1.4}$ kpc from the Sun, ~ 1 kpc below the Galactic plane near the Galactic center, shows two high-velocity H_2 components at $v_{\text{LSR}} = -79$ and -108 km s^{-1} . In contrast, the FUSE spectrum of the nearby ($\sim 0.6^\circ$ away) foreground star HD 167402 at $d = 4.9_{-0.7}^{+0.8}$ kpc reveals no H_2 absorption at these velocities. Over 60 lines of H_2 from rotational levels $J = 0$ to 5 are identified in the high-velocity clouds. For the $v_{\text{LSR}} = -79 \text{ km s}^{-1}$ cloud we measure total $\log N(\text{H}_2) \geq 16.75 \text{ cm}^{-2}$, molecular fraction $f_{\text{H}_2} \geq 0.8\%$, and $T_{01} \geq 97$ and $T_{25} \leq 439 \text{ K}$ for the ground- and excited-state rotational excitation temperatures. At $v_{\text{LSR}} = -108 \text{ km s}^{-1}$, we measure $\log N(\text{H}_2) = 16.13 \pm 0.10 \text{ cm}^{-2}$, $f_{\text{H}_2} \geq 0.5\%$, and $T_{01} = 77_{-18}^{+34}$ and $T_{25} = 1092_{-117}^{+149} \text{ K}$, for which the excited-state ortho- to para- H_2 is $1.0_{-0.1}^{+0.3}$, much less than the equilibrium value of 3 expected for gas at this temperature. This nonequilibrium ratio suggests that the -108 km s^{-1} cloud has been recently excited and has not yet had time to equilibrate. As the LS 4825 sight line passes close by a tilted section of the Galactic disk, we propose that we are probing a boundary region where the nuclear wind is removing gas from the disk.

Unified Astronomy Thesaurus concepts: Galactic center (565); Galactic winds (572); Molecular gas (1073); Ultraviolet astronomy (1736)

1. Introduction

The Galactic center (GC) is host to the Milky Way's (MW) nuclear wind, powered by the supermassive black hole Sagittarius A* and surrounding regions of intense star formation. Evidence for the nuclear activity comes from multiple sources, the most notable being the Fermi (Su et al. 2010; Ackermann et al. 2014) and eROSITA Bubbles (Bland-Hawthorn & Cohen 2003; Predehl et al. 2020), giant gamma- and X-ray lobes extending ~ 10 kpc above and below the Galactic plane (see Figure 1), which outline the present boundaries of the wind (see also Sofue & Kataoka 2021). Additional evidence is provided by an H I outflow, seen in the form of several hundred hydrogen 21 cm clouds (McClure-Griffiths et al. 2013; Di Teodoro et al. 2018; Lockman et al. 2020) detected at low latitude within the Fermi Bubbles. Finally, ultraviolet (UV) absorption-line studies reveal high-velocity absorption in low-ionization (e.g., C I, O I, S II) and high-ionization (e.g., C IV, Si IV) species in sight lines through the Fermi Bubbles. These UV absorbers trace outflowing gas that spans an extremely large range in physical conditions (Keeney et al. 2006; Zech et al. 2008; Fox et al. 2015; Bordoloi et al. 2017; Savage et al. 2017;

Karim et al. 2018; Ashley et al. 2020). Nuclear outflow is also detected in H α emission (see Krishnarao et al. 2020a).

Together these observations suggest that a multiphase nuclear outflow exists, with neutral, warm ionized, and highly ionized components. But until now, very little information on *molecular* gas in the nuclear outflow has existed, with the only information being from two CO emission-line clouds reported by Di Teodoro et al. (2020) and no detection in near-IR H_2 emission lines (Fox et al. 2021). ALMA observations toward J1744-3116 show millimeter-wave molecular absorption (HCO^+ , HCN, CS) at velocities arising inside the Galactic bulge near the GC (Liszt & Gerin 2018).

High-velocity molecular gas is rarely detected *anywhere* in the Galactic halo, not just the GC. The only UV absorption-line detections of H_2 in high-velocity clouds (HVCs) are by Richter et al. (1999, 2001), Sembach et al. (2001), and Wakker (2006), with low molecular fractions $f(\text{H}_2) \sim 10^{-6}$ – 10^{-2} .

In this paper, we present the first detection of H_2 associated with the MW nuclear wind from analysis of archival spectra of two closely spaced low-latitude stars, LS 4825 and HD 167402, observed by the Far-Ultraviolet Spectroscopic Explorer (FUSE; Moos et al. 2000). At low latitudes close to the GC, tracing the nuclear outflow is complicated by irregularities in the shape of the Galactic disk (Liszt & Burton 1980; Krishnarao et al. 2020b), which make the disk/wind separation nontrivial. The sight lines lie in close proximity to a warped portion of the Galactic disk,

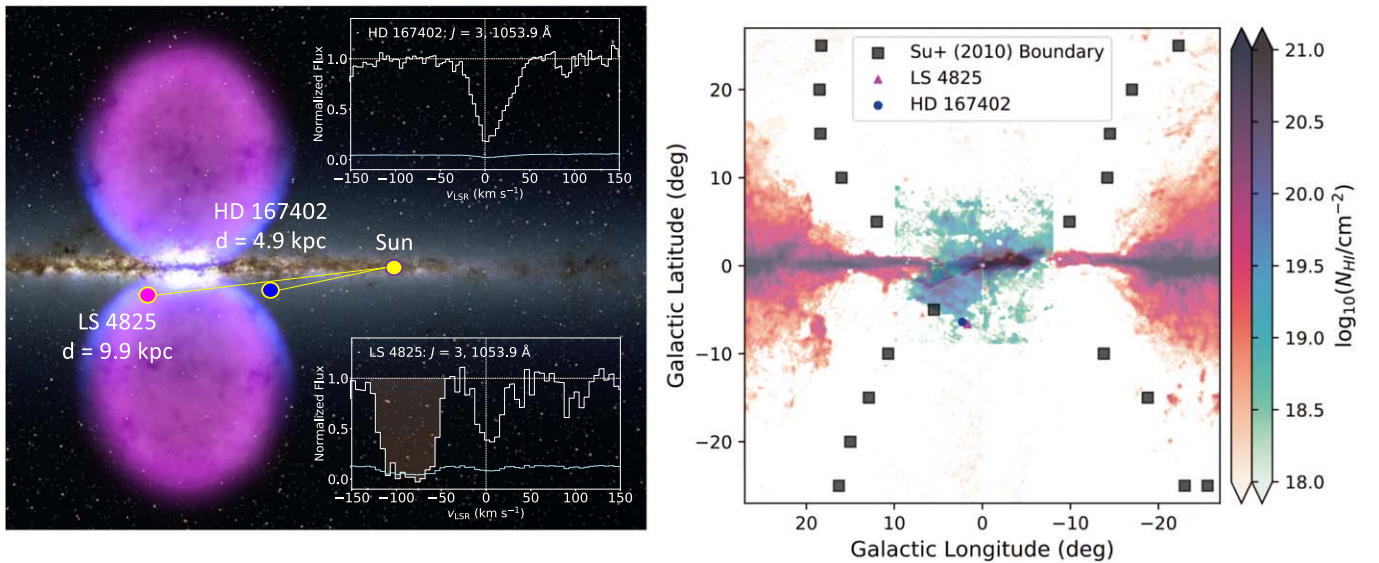


Figure 1. (Left) Edge-on depiction of the Galaxy, with the positions of LS 4825 and HD 167402 marked at their Gaia EDR3 distances of 9.9 and 4.9 kpc, respectively, from the Sun. The purple symmetric lobes show the Fermi Bubbles (image adapted from NASA’s Goddard Space Flight Center). The blue edges of the lobes show X-ray emission from ROSAT (Bland-Hawthorn & Cohen 2003). The inset panels show the absorption profiles of H₂ $J = 3$ 1053.9 Å, one of over 60 lines of H₂ detected in the FUSE spectra. The vertical line at 0 km s⁻¹ marks absorption associated with the MW. The strong absorption shaded in orange near -100 km s⁻¹ in the background spectrum of LS 4825 is not present in the foreground spectrum of HD 167402, thus bracketing the absorbing region to 4.9 < d < 9.9 kpc. (Right) 21 cm HI emission map from the GASS survey showing the HI column density at the Galactic tangent points (red scale) from Lockman & McClure-Griffiths (2016) and at velocities anomalous to circular rotation which track the tilt of the disk near the Galactic center (green-scale: left half from -110 to -70 km s⁻¹, right half from +70 to +110 km s⁻¹). The black squares denote the gamma-ray boundaries of the Fermi bubbles from Su et al. (2010). The foreground FUSE sight line toward HD 167402 at $d = 4.9$ kpc is marked with a blue circle and the background sight line toward LS 4825 at $d = 9.9$ kpc is marked with a magenta triangle.

indicating that we may be probing an interface between the disk and the nuclear wind.

2. H₂ Data and Measurements

LS 4825 is a B1 Ib–II blue supergiant with extinction $E(B - V) = 0.24$ (Savage et al. 2017, hereafter S17) located at $l, b = 1.67^\circ, -6.63^\circ$. HD 167402, a B0 Ib supergiant with $E(B - V) = 0.23$ (Shull & Danforth 2019), lies $\sim 0.6^\circ$ away at a maximum projected distance of ~ 50 pc, at $l, b = 2.26^\circ, -6.39^\circ$. Ryans et al. (1997) measured a spectroscopic distance of 21 ± 5 kpc for LS 4825, though recent Gaia EDR3 astrometry measurements (Bailer-Jones et al. 2021) place LS 4825 at a much closer distance of $9.9^{+1.4}_{-0.8}$ kpc. HD 167402 has multiple estimates of its spectrophotometric distance, with S17 reporting 7.0 ± 1.7 kpc and Shull & Danforth (2019) finding 7.6 kpc (see also Shull et al. 2021). Gaia EDR3 reports $d = 4.9^{+0.8}_{-0.7}$ kpc for HD 167402. We adopt the Gaia distances in our analysis. Through comparative analysis of the foreground HD 167402 and background LS 4825 sight lines, we isolate absorption from the interval $5 \lesssim d \lesssim 10$ kpc assuming that the ISM coherence length is larger than the projected separation.

FUSE observations of LS 4825 and HD 167402 were performed on 2000 August 29 under program ID P101 (PI: K. Sembach). The raw spectra were obtained from the FUSE archive, and the CalFUSE pipeline (v3.2.1, Dixon & Kruk 2009) was used to extract the spectra. The SiC channels ($\lambda < 1000$ Å) show complex, overlapping absorption and low signal-to-noise (S/N) ratios and were not used for the analysis. Instead we focus on the spectra from the LiF1 and LiF2 channels, which have $S/N \sim 9$ –13 per resolution element and a velocity resolution of 20 km s⁻¹ (FWHM). The data were binned by three pixels for the fitting analysis. A detailed explanation of refinements to the CalFUSE data reduction

procedures can be found in Wakker et al. (2003) and Wakker (2006).

The FUSE spectrum of LS 4825 shows high-velocity H₂ absorption in over 60 distinct lines from the rotational levels $J = 0, 1, 2, 3, 4,$ and 5 (see Figure 2). Two components are seen at $v_{\text{LSR}} = -79.4 \pm 1.5$ and -107.6 ± 1.3 km s⁻¹. Both components have high deviation velocities (Wakker 1991), thus we label both as HVCs even though the -79 km s⁻¹ component is below the commonly used HVC threshold of $|v| = 90$ km s⁻¹. The spectrum of LS 4825 is complex due to its spectral type (B1 Ib–II), and the stellar continuum placement was guided by reference to the behavior of the FUSE spectrum of the comparison star HD 58510 (FUSE program ID P102; PI: K. Sembach). HD 58510 has the identical spectral type (S17) and tracks the continuum of LS 4825 closely, with similar zero-velocity H₂ absorption but without the high-velocity H₂ absorption. The continua were normalized in local regions of interest using `linetools` (Prochaska et al. 2017).

We used the VPFIT (v12.2, Carswell & Webb 2014) Voigt-profile-fitting software to simultaneously fit the individual HVC components for the $J = 4$ and 5 transitions, as these transitions are unsaturated. Since the two HVC components in the lower- J -levels ($J < 4$) show significant blending, we assume the velocity centroid and b -value derived from $J = 4$ and 5 (see Table 1) apply to the $J < 4$ levels. There is some evidence that b -values of interstellar H₂ may vary as a function of J (Spitzer & Morton 1976; Jenkins & Peimbert 1997), but because of saturation we are unable to determine whether this is the case in our data set. Jensen et al. (2010) performed a study on a sample of 22 Galactic sight lines to determine the effects of assuming a uniform b -value for $J \geq 2$ versus independent measurements and overall found $\log N(\text{H}_2)$ differences < 0.07 dex for the excited states. We quantify the effect this may have on our $J < 4$ column densities (including $J = 0$ and 1) by

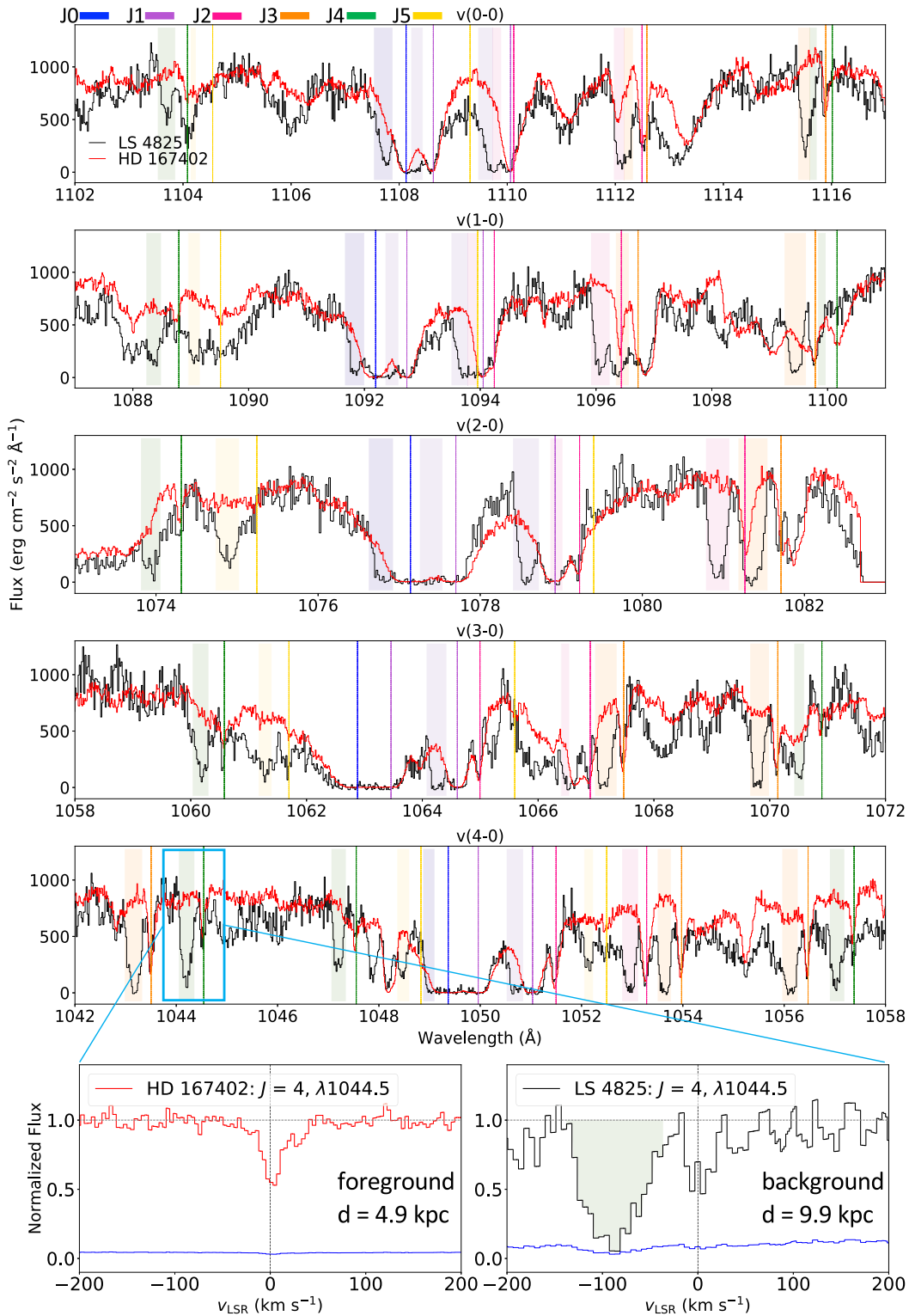


Figure 2. FUSE spectra of LS 4825 (background star; black) and HD 167402 (foreground star; red) showing five vibrational H_2 bands, each of which has rotational substructure. The LS 4825 spectrum has been multiplied by the average flux ratio of the two stars in the corresponding region to facilitate the comparison. Absorption associated with MW for J -levels 0, 1, 2, 3, 4, and 5 are marked in the panels with blue, purple, pink, orange, green, and yellow vertical lines, respectively. The shaded bands mark the region of the HVCs in the background spectrum. The bottom two side-by-side panels show separate radial velocity plots of the normalized data for the $J = 4$ 1044 Å transition to illustrate the difference between the background and foreground spectra, where the vertical line at 0 km s^{-1} marks absorption associated with the MW, and the 1σ error in the normalized flux is shown in blue. The HD 167402 (foreground) spectrum only shows H_2 absorption associated with the MW near 0 km s^{-1} . The LS 4825 (background) spectrum shows additional strong multi-component H_2 absorption centered near -100 km s^{-1} .

Table 1
HVC Molecular Absorption-Line Measurements

Species $\nu_u-\nu_l$, R/P(J_l)	λ_{rest} (Å)	f^a	$\log N(\text{H}_2)_{v=-79}^b$ (N in cm^{-2})	$\log N(\text{H}_2)_{v=-108}^c$ (N in cm^{-2})
H₂ $J = 0$				
0 – 0, R(0)	1108.1273	1.66×10^{-3}	16.01 ± 0.25	15.63 ± 0.27
1 – 0, R(0)	1092.1952	5.78×10^{-3}		
2 – 0, R(0)	1077.1387	1.17×10^{-2}		
H₂ $J = 1$				
1 – 0, P(1)	1094.0519	1.97×10^{-3}	>16.20	15.62 ± 0.12
2 – 0, P(1)	1078.9255	3.92×10^{-3}		
4 – 0, P(1)	1051.0325	7.60×10^{-3}		
H₂ $J = 2$				
2 – 0, P(2)	1081.2660	4.70×10^{-3}	>16.15	15.28 ± 0.08
3 – 0, P(2)	1066.9007	7.09×10^{-3}		
4 – 0, P(2)	1053.2843	9.02×10^{-3}		
H₂ $J = 3$				
3 – 0, P(3)	1070.1409	7.54×10^{-3}	>16.13	15.15 ± 0.11
3 – 0, R(3)	1067.4786	1.00×10^{-2}		
5 – 0, P(3)	1043.5032	1.08×10^{-2}		
4 – 0, R(3)	1053.9761	1.34×10^{-2}		
H₂ $J = 4$				
3 – 0, P(4)	1074.3130	7.74×10^{-3}	15.08 ± 0.05	14.99 ± 0.06
5 – 0, P(4)	1047.5519	1.10×10^{-2}		
4 – 0, R(4)	1057.3807	1.29×10^{-2}		
5 – 0, R(4)	1044.5433	1.55×10^{-2}		
H₂ $J = 5$				
3 – 0, R(5)	1075.2441	9.28×10^{-3}	14.95 ± 0.05	14.81 ± 0.06
5 – 0, P(5)	1052.4970	1.11×10^{-2}		
Total $\log N(\text{H}_2)$			>16.75	16.13 ± 0.10
H I (S17) ^d	21 cm	...	19.43 ± 0.15	18.28 ± 0.15
H I (this work) ^e	21 cm	...	19.14 ± 0.16	< 18.77
f_{H_2} (S17) ^f			$>0.41\%$	$1.40 \pm 0.26\%$
f_{H_2} (this work) ^g			$>0.81\%$	$>0.46\%$

Notes.

^a The wavelengths and oscillator strengths used by VPFIT are calculated from Bailly et al. (2010).

^b The b -value from VPFIT for this component is $14.9 \pm 1.7 \text{ km s}^{-1}$.

^c The b -value from VPFIT for this component is $11.7 \pm 1.5 \text{ km s}^{-1}$.

^d S17 determine $\log N_{\text{HI}} = 19.43 \pm 0.01$ and 18.28 ± 0.02 for the -79 and -108 km s^{-1} components in the 21 cm data from the Green Bank Telescope (GBT, program ID: 14B-299). The $\log N_{\text{HI}}$ errors include a beam smearing error of ± 0.15 since we are combining the GBT data ($9'1$ beam) with the FUSE UV measurements (infinitesimal beam) to derive f_{H_2} .

^e Revised estimate of $\log N_{\text{HI}}$ from a refit to the GBT LS 4825 spectrum in S17 where the MW foreground H₂ absorption of HD 167402 has been subtracted. The $\log N_{\text{HI}}$ error for the $v = -79 \text{ km s}^{-1}$ component includes a beam smearing error of ± 0.15 .

^f The molecular fraction, $f_{\text{H}_2} = 2N(\text{H}_2)/[N(\text{H I}) + 2N(\text{H}_2)]$, based on $\log N_{\text{HI}}$ from S17.

^g Estimate of the molecular fractions derived from the revised multi-component refit to the 21 cm H I GBT spectrum in S17.

lowering b by 3 km s^{-1} , as any larger reduction in b results in fits that overfit the profile. For weak unsaturated transitions we find that $\log N(\text{H}_2)$ at -79 and -108 km s^{-1} increases by at most 0.04 dex.

We denote the resulting total column density for a component of a given J -level as a lower limit if the profile of the *weakest* (lowest f -value) transition in the set of simultaneously fit lines reaches zero flux. H₂ lines blended with ISM metal lines were excluded from fitting, as were lines blended with other H₂ lines and those in regions of geocoronal emission. All lines of a single J -level were visually inspected in velocity space to verify that when progressing from weakest

to strongest lines the absorption behaved as expected, and to check for the presence of damping wings on the HVC H₂ components. Following continuum reconstruction using the reference star and the adoption of a two-component fit, we find no evidence for HVC damping wings. This is also consistent with the very small differential extinction between the foreground and background sight lines using $E(B - V)$ values reported in S17 and Shull & Danforth (2019), $\Delta E(B - V) = 0.01$, because this indicates a similar total dust column and therefore similar total hydrogen column in the two directions.

We employed a slightly different procedure to fit the HVC ground state $J = 0, 1$ components due to overlapping with

strong Milky Way (MW) foreground H_2 absorption. For these lines we fit a Voigt profile to the MW H_2 component with fixed $b = 5.5 \text{ km s}^{-1}$ and adjusted its column density interactively until the profile best fit the damping wings for all selected lines of the given J -level. The choice of $b = 5.5 \text{ km s}^{-1}$ was motivated by published high-resolution ($\text{FWHM} = 6.6 \text{ km s}^{-1}$) STIS observations of C I toward LS 4825 (S17), where $b_{\text{CI}} = 5.4 \text{ km s}^{-1}$ at $T \sim 100 \text{ K}$ indicates that the gas is almost fully turbulent. The velocity, b -value, and column density of the MW foreground component were then held fixed, and the column density for the HVC components was then determined as described above for the excited J -levels. The resulting Voigt profile fits to the H_2 lines are shown in Figure 3 and the resulting velocities, b -values, and column densities are shown in Table 1.

3. Results

Our most significant result is the discovery of the presence of the high-velocity H_2 absorption in two components in the spectrum of the background star LS 4825, centered at -79 and -108 km s^{-1} . This remains true irrespective of our detailed findings on column densities and rotational excitations discussed below. The high-velocity H_2 components are not seen in the spectrum of the foreground star HD 167402, indicating that the H_2 detected at -79 and -108 km s^{-1} in the background star LS 4825 can be bracketed to the range $5 \lesssim d \lesssim 10 \text{ kpc}$, which corresponds to a z -distance of -0.6 to -1.2 kpc below the GC. The H_2 is therefore potentially associated with the southern Fermi Bubble, a region exposed to the Galactic nuclear wind.

The absence of high-velocity absorption toward HD 167402 was also seen in the STIS E140M and E230M UV spectrum by S17, who reported multiphase gas at high velocities only in the LS 4825 spectrum. Low-ion absorption is seen over the range -290 to 94 km s^{-1} . Of particular significance is C I absorption detected at $v_{\text{LSR}} = -114.2, -100.8,$ and -77.7 km s^{-1} in the STIS spectrum (S17) because C I acts as a tracer for H_2 (Ge et al. 1997, 2001). The combination of our results from H_2 detected at similar velocities with those from S17 allows us to construct a more complete picture of the composition, properties, and environment of these cold clouds in the dynamic environment near the GC.

3.1. The H_2 HVC at -79 km s^{-1}

By summing over the rotational levels from $J=0$ to 5, we derive a total H_2 column density in the -79 km s^{-1} component of $\log N(\text{H}_2) > 16.75 \text{ cm}^{-2}$. This is a lower limit due to saturation in multiple J -levels. S17 report HI 21 cm emission at negative velocities of $-105, -89,$ and -70 km s^{-1} using a Green Bank Telescope (GBT) spectrum and conclude that the -70 km s^{-1} component with $\log N_{\text{HI}} = 19.43 \pm 0.01$ is most likely associated with the absorption system near -78 km s^{-1} . Combining this HI measurement with our measurement of $\log N(\text{H}_2)$ we derive a molecular fraction of $f_{\text{H}_2} = 2N(\text{H}_2)/[N(\text{H I}) + 2N(\text{H}_2)] \geq 4.1 \times 10^{-3}$, or $\geq 0.41\%$ (see Table 1). We conducted a refit to the LS 4825 GBT spectrum, in which we subtracted the zero-velocity component of the foreground HD 167402 spectrum. This results in two components at -85.8 and -62.3 km s^{-1} with $\log N_{\text{HI}} = 19.14 \pm 0.16$ and $19.07 \pm 0.16 \text{ cm}^{-2}$, respectively. We associate the HI emission near -86 km s^{-1} with the H_2 absorption at -79 km s^{-1} and find $f_{\text{H}_2} \geq 0.81\%$.

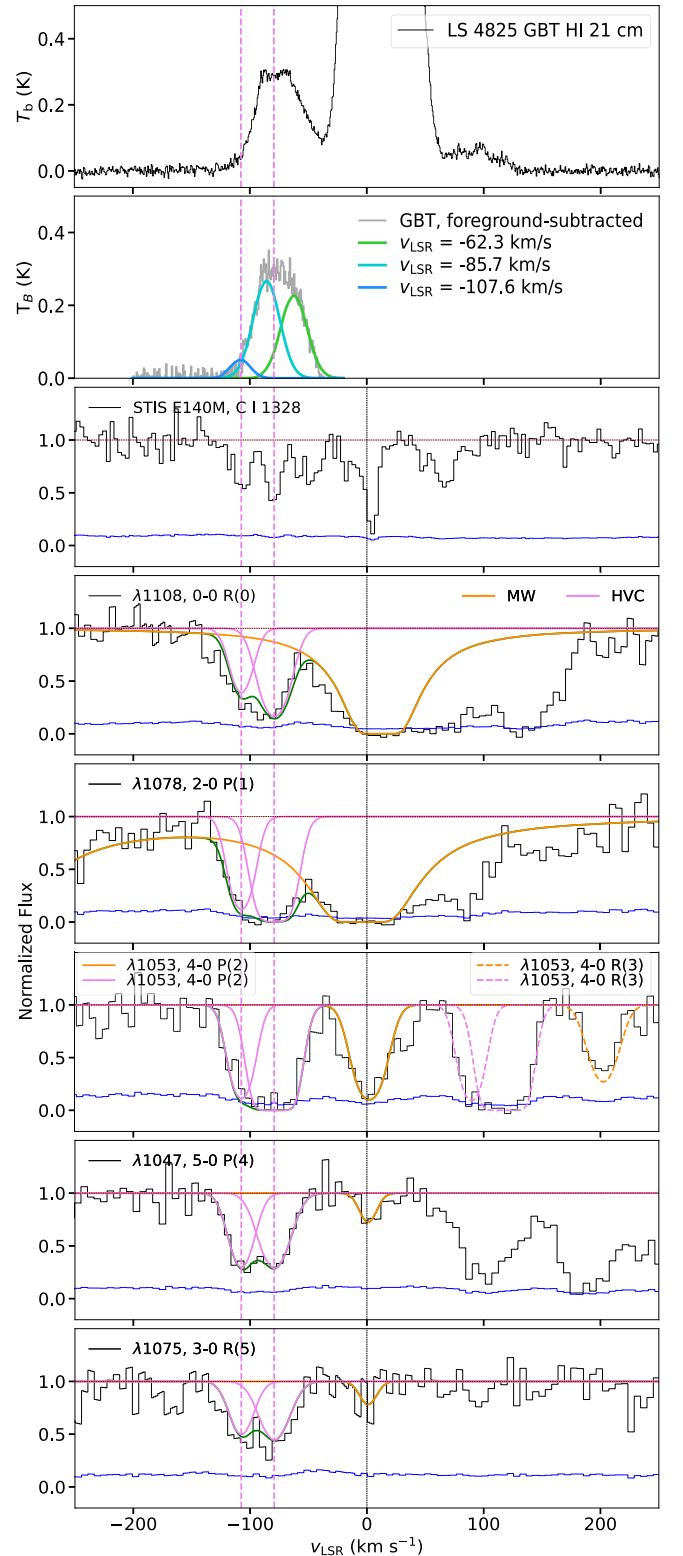


Figure 3. Velocity profiles of H_2 absorption lines and HI emission toward LS 4825. Panel 1: LS 4825 21 cm GBT spectrum from S17. Panel 2: refit to the MW foreground-subtracted spectrum with $\log N_{\text{HI}} = 19.14 \pm 0.16$ at -86 km s^{-1} and ≤ 18.77 at -108 km s^{-1} . Panel 3: closely aligned H_2 from this work with C I from S17. Panels 4–8: a sample of H_2 absorption lines for rotational levels $J = 0$ –5. The normalized flux is shown in black, the continuum level is in red, and the 1σ error in the normalized flux is in blue. The vertical line at 0 km s^{-1} marks the region associated with the MW. The solid orange and magenta curves are Voigt profile fits to the H_2 absorption features for the MW and the HVCs, respectively. In all panels, the two vertical dashed magenta lines indicate the velocities of the HVC components.

Either limit is consistent with the upper end of $f_{\text{H}_2} = 10^{-2} - 10^{-6}$ measured in Galactic HVCs from absorption-line studies (Richter et al. 2001; Sembach et al. 2001; Wakker 2006), but is not as high as $f_{\text{H}_2} \sim 0.3 - 0.6$ from emission-line CO detections seen in Di Teodoro et al. (2020).

We determine limits on the excitation temperatures in the high-velocity molecular gas by fitting a theoretical Boltzmann distribution to the observed population of rotational levels, since our measurements of $\log N(\text{H}_2)$ for $J = 1, 2, 3$ are lower limits. For the -79 km s^{-1} component, the rotational ground states $J = 0$ and 1 are fit by a slope equivalent to a Boltzmann temperature $T_{01} \geq 97 \text{ K}$, whereas the excited rotational levels $J = 2 - 5$ fit on a slope equivalent to $T_{25} \leq 439 \text{ K}$ (see Figure 4). The adopted two-slope solution may suggest a core-envelope structure, with T_{01} reflecting the temperature in the cooler, shielded interior of the cloud and the T_{25} region tracing warmer gas heated by processes such as UV pumping, H_2 formation pumping, and shock excitation (Richter et al. 2001). However, these processes could occur within a fairly homogeneous region.

S17 measure a near solar metallicity $[\text{S}/\text{H}] = 0.02 \pm 0.16$ in the -78 km s^{-1} HVC ($[\text{S}/\text{H}] = 0.31 \pm 0.17$ using the H I measurement from the foreground-subtracted GBT spectrum), and also report a subsolar Fe/S ratio, finding $[\text{Fe II}/\text{S II}] = -1.05 \pm 0.05$, which suggests that Fe in the cloud is locked up in dust grains.

3.2. The H_2 HVC at -108 km s^{-1}

We report $\log N(\text{H}_2) = 16.13 \pm 0.10 \text{ cm}^{-2}$ for the -108 km s^{-1} component, 0.6 dex lower than the H_2 column at -79 km s^{-1} . From the MW foreground-subtracted GBT spectrum of LS 4825 we determine a 3σ upper limit of $\log N_{\text{HI}} \leq 18.77$ at -107.6 km s^{-1} , which is ~ 0.5 dex higher than S17, who measure $\log N_{\text{HI}} = 18.28 \pm 0.02$ at -104.9 km s^{-1} . Combining the H I and H_2 columns results in $f_{\text{H}_2} \geq 0.46\%$, which is also consistent with the upper end of f_{H_2} for HVCs in absorption-line studies (see Section 3.1). The metallicity $[\text{S}/\text{H}] \geq 0.87$ is supersolar; and S17 measure $[\text{Fe II}/\text{S II}] = -0.99 \pm 0.09$ for this component, concluding that it is as equally dusty as the -79 km s^{-1} component.

A two-slope solution for the Boltzmann distribution fit to the rotational level populations yields $T_{01} = 77^{+34}_{-18} \text{ K}$ and $T_{25} = 732^{+64}_{-55} \text{ K}$, as determined from the dark blue lines in Figure 4, but is not a good fit for the $J \geq 2$ excited states. However, the up-and-down distribution of the excited states, in which the para states $J = 2, 4$ lie systematically above the ortho states $J = 3, 5$ may indicate an ortho-to-para ratio (OPR) that deviates from the canonical (equilibrium) value of 3 for warm, rotationally excited H_2 gas (as included in the statistical weight, g_J , where $g_J(\text{para}) = 2J + 1$ and $g_J(\text{ortho}) = 3(2J + 1)$). If we adjust the OPR for $J \geq 2$ to a value of 1 ($^{+0.3}_{-0.1}$) instead of 3, the data points for $J = 3, 5$ (in light blue) are shifted higher such that all $J \geq 2$ levels fit on a straight line, with a slope that yields $T_{\text{exc}} = 1092^{+149}_{-117} \text{ K}$ (see Figure 4). This suggests that the OPR is out of equilibrium and is further discussed in Section 4. An OPR = 1 provides a good fit to the data for the excited states of the -108 km s^{-1} component, however, we acknowledge that unresolved components with potentially varying b -values could impact the measurements of the excited-state column densities. These fits represent what is currently capable given the resolution of the data.

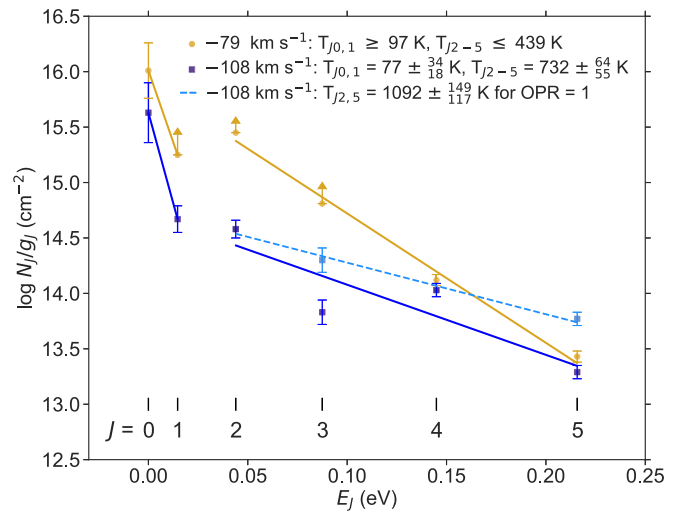


Figure 4. Boltzmann excitation plot for the two high-velocity H_2 components toward LS 4825. The H_2 column density in each rotation level N_J divided by the level's statistical weight g_J is plotted as a function of excitation energy (E_J) for each cloud, for $J = 0 - 5$. The HVCs at -79 and -108 km s^{-1} are indicated with gold circles and blue squares, respectively. For the cloud at -79 km s^{-1} , we adopt a two-slope solution to describe the relative population of the ground-state ($J = 0, 1$) and excited-state levels ($J = 2 - 5$), as indicated in the legend. For the cloud at -108 km s^{-1} , we also consider a model in which the ortho-to-para ratio (OPR) of the excited-state levels is 1 instead of 3, which would shift $\log N_J/g_J$ for $J = 3, 5$ upward to the positions indicated by the light blue squares and for which the light blue dashed line is a better fit to the distribution of points.

4. Discussion

The H_2 components detected in the FUSE spectrum of LS 4825 ($d = 9.9^{+1.4}_{-0.8} \text{ kpc}$) at -79 and -108 km s^{-1} are not seen in the spectrum of the foreground star HD 167402 ($d = 4.9^{+0.8}_{-0.7} \text{ kpc}$) and therefore trace gas located between the two stars and most likely within the southern Fermi Bubble (see Figure 1). Our results represent the first detection of high-velocity H_2 in the extended Galactic center environment. We measure total $\log N(\text{H}_2) > 16.75$ and $16.13 \pm 0.10 \text{ cm}^{-2}$ at -79 and -108 km s^{-1} respectively, velocities which cannot be explained by circular rotation. We determine respective H_2 fractions $f_{\text{H}_2} \geq 0.8\%$ and $f_{\text{H}_2} \geq 0.5\%$. The low ground-state temperatures we derive for the H_2 absorption at -79 and -108 km s^{-1} of $T_{01} \approx 97$ and 77 K confirm that these are indeed cold clouds. The H_2 detection augments the metal-line analysis from S17, who reported high-velocity neutral, low-ion, and high-ion absorption toward LS 4825 but not HD 167402.

A natural interpretation of these results, as suggested by S17, is that the multiphase high-velocity absorbers toward LS 4825 trace a nuclear wind. This is supported by the very strong high-ion absorption seen along the line of sight (S17) and the abundant multi-wavelength evidence for a wind in this region (Bland-Hawthorn & Cohen 2003; Su et al. 2010; Di Teodoro et al. 2018; Lockman et al. 2020; Predehl et al. 2020). In this interpretation, only a small component of the outflow velocity is projected along our line of sight; deprojecting the velocity onto a vertically or radially oriented outflow implies a high outflow velocity ($\sim 800 - 1000 \text{ km s}^{-1}$), similar to the velocity inferred from other UV HVCs in the Fermi Bubbles (Fox et al. 2015; Bordoloi et al. 2017).

However, multiple structures house molecular and neutral gas in the GC. The Galactic disk near the GC is warped, tilted at $\sim 22^\circ$ (Liszt & Burton 1980) with a portion protruding to

$b \sim -5^\circ$ between $l = 0-10^\circ$ (as shown in Figure 1). Recent H α studies at the anomalous velocities that track the tilt of the Galactic disk in this region from Krishnarao et al. (2020b) predict asymmetric absorption profiles with peak absorption near -100 km s^{-1} , just as we observe. Even closer to the GC lies the central molecular zone inside $R_G \sim 0.5 \text{ kpc}$. The right panel of Figure 1 shows that the sight lines lie in close proximity to the edge of the disk and could be probing the boundary where the nuclear wind is passing by the disk since the HVCs and the disk have similar velocities in this inner region. Irrespective of whether the clouds are entrained in an escaping wind, we see strong evidence of disk-like properties for the molecular components from their high metallicities, including an above-solar $[S/H] = 0.31 \pm 0.17$ at -79 km s^{-1} and a supersolar $[S/H] \geq 0.87$ near -108 km s^{-1} , as well as high dust depletion levels, with $[\text{Fe II}/\text{S II}] \sim -1$ (S17).

Both the wind interpretation and the warped-disk interpretation are allowed by the data. However, the two are not mutually exclusive. We propose a hybrid model in which the high-velocity H $_2$ clouds probe a boundary region where the nuclear wind is passing by the disk and accelerating fragments of gas into the halo. This is supported by the sight line's close proximity to the disk (both spatially and kinematically), as well as unusual OPRs and thermal pressures (S17), as we explain below.

Warm, rotationally excited H $_2$ gas in thermal equilibrium is expected to have an OPR = 3, as the excited gas has been warm for long enough to reach equilibrium between the (odd) ortho and (even) para states. As seen in Figure 4, an OPR = 3 is a good description of the distribution of excited-state levels for the cloud at -79 km s^{-1} . However, as described in Section 3, an OPR = 3 fails to describe the excited J-levels for the -108 km s^{-1} cloud, which instead is much better fit by OPR = 1. This deviation from the canonical (equilibrium) value suggests that the observed $J = 2-5$ levels at -108 km s^{-1} were only recently pumped into high J states (and also to higher T) from the ground states ($J = 0$ and 1), where $\text{OPR} \lesssim 1$ is expected (Flower & Watt 1984). The OPR equilibrates very slowly (Neufeld et al. 1998), so in this explanation the excited-state gas has not had enough time to adjust to the new environment to reach equilibrium between the ortho and para states, and so preserves a ‘‘memory’’ of the thermal state of gas in a previous epoch. We note that an enhanced radiation field within the Fermi Bubbles is *predicted* in the models of Bland-Hawthorn et al. (2019), who find an ionizing radiation field of $\log \varphi = 6.5$ photons $\text{cm}^{-2} \text{ s}^{-1}$ at $\sim 1 \text{ kpc}$ below the GC, and potentially higher in the event of a recent Seyfert flare. The unusual H $_2$ excitation properties we observe are consistent with this.

In the hybrid scenario, the two H $_2$ clouds $\sim 1 \text{ kpc}$ below the GC undergo different histories. Both clouds formed much earlier in a quiescent disk environment at $T < 100 \text{ K}$ and were swept and/or broken up within the nuclear wind. In this new environment, the outer skin of the clouds was rotationally excited by photons and/or collisions with an ambient medium. Whereas the -79 km s^{-1} cloud has equilibrated to this environment with $T_{\text{exc}} \approx 492 \text{ K}$ for OPR = 3, the -108 km s^{-1} cloud has not, as evidenced by $T_{\text{exc}} = 1092 \text{ K}$ with an OPR = 1 that still reflects the physical conditions of the H $_2$ gas from its prior environment.

Further support for a wind or hybrid model is provided by the high thermal pressure in the HVCs. From observations of $N(\text{C I})$, $N(\text{C I}^*)$, and $N(\text{C I}^{**})$, S17 derive thermal pressures P/k

at -78 , -101 , and -114 km s^{-1} of $\sim 10^{4.1}$, $10^{3.8}$, and $10^5 \text{ cm}^{-3} \text{ K}$, respectively. The pressures reported at -78 and -114 are ~ 3.2 and 25 times higher than the mean $P/k = 10^{3.6 \pm 0.2} \text{ cm}^{-3} \text{ K}$ reported in the diffuse ISM in the Galactic disk (Jenkins & Tripp 2011), which suggests that the clouds may have been compressed, perhaps by an outflowing hot wind. The pressure at -101 km s^{-1} , however, is similar to the mean ISM cloud pressure. Since we measure an H $_2$ velocity centroid in the lower resolution FUSE spectrum at -108 km s^{-1} , we are unable to make a confirmed association with either of the STIS components at -101 and -114 km s^{-1} , but acknowledge that the range of pressures observed near this velocity are consistent with a hybrid disk-wind environment along this line of sight.

If the clouds are indeed being actively swept out of the disk, perhaps in a biconical outflow from the GC (see Fox et al. 2015; Bordoloi et al. 2017), then questions arise on how the cold gas became entrained and will survive in this complex and energetic environment. HVCs are thought to have a finite lifetime against disruptive instabilities as they interact with a surrounding medium (Heitsch & Putman 2009; Armillotta et al. 2017). However, recent theoretical studies have explored the survival of cold gas in hot galactic winds (e.g., Gronke & Oh 2020; Sparre et al. 2020). They indicate that a cold gas cloud entrains hot gas via cooling-induced pressure gradients, thereby acquiring the mass and momentum of the hot gas. Inclusion of a magnetic field, and in particular, a turbulent magnetic wind, can suppress the cloud-destroying Kelvin-Helmholtz instabilities, allowing the clouds to survive. These models show that clouds with $N_{\text{H}} < 10^{18} \text{ cm}^{-2}$ are not predicted to survive due to erosion, whereas those with $N_{\text{H}} > 10^{18} \text{ cm}^{-2}$ are expected to survive and even grow.

The results of these models offer a plausible explanation for how the low column density H $_2$ components may survive, as comoving within clouds with $N_{\text{H}} > 10^{18} \text{ cm}^{-2}$ could possibly shield the H $_2$ bearing structures, ensuring their survival. If entrained in a wind, the existence of these high-velocity molecular clouds in the dynamic and multiphase GC environment will help to inform continuing research on models of cloud acceleration and survival. However, further detections of molecular gas at more locations within the nuclear wind are needed to test these theories.

5. Summary

We have detected two high-velocity molecular hydrogen clouds in the FUSE spectrum of the massive star LS 4825. The sight line passes $\sim 1 \text{ kpc}$ below the GC near the boundary of the Galactic disk, a region where the nuclear wind is thought to blow gas out into the southern Fermi Bubble. The clouds are not seen in the spectrum of the foreground star HD 167402, lying $\sim 0.6^\circ$ away, confirming they are associated with the GC. We measure total $\log N(\text{H}_2) > 16.75$ and $16.13 \pm 0.10 \text{ cm}^{-2}$ at -79 and -108 km s^{-1} respectively, velocities which cannot be explained by circular rotation. We determine respective H $_2$ fractions $f_{\text{H}_2} \geq 0.8\%$ and $f_{\text{H}_2} \geq 0.5\%$. For the -79 km s^{-1} cloud we adopt a two-component Boltzmann distribution to explain the rotational level populations, with $T_{01} \geq 97 \text{ K}$ and $T_{25} \leq 439 \text{ K}$. For the -108 km s^{-1} cloud, a two-component Boltzmann distribution yields $T_{01} = 77_{-18}^{+34}$ and $T_{25} = 732_{-55}^{+64} \text{ K}$, but is not a good fit for the excited states given the canonical OPR = 3. Instead we find that if OPR = 1, the excited states lie on a straight line corresponding to $T_{25} = 1092_{-117}^{+149} \text{ K}$.

We considered two possible origins for the high-velocity H₂ components: a wind interpretation which traces the projection of an outflow velocity along our line of sight, and a warped-disk interpretation in which the clouds are associated with the tilted portion of the Galactic disk. We conclude that the best explanation for the data is a hybrid model in which the H₂ clouds probe a boundary region where the nuclear wind is passing by the disk and accelerating fragments of gas into the halo.












We thank Enrico Di Teodoro for valuable conversations on the LS 4825 sight line and Stephen McCandliss for helpful conversations about molecular absorption lines. We gratefully acknowledge support from the NASA Astrophysics Data Analysis Program (ADAP) under grant 80NSSC20K0435, 3D Structure of the ISM toward the Galactic Center. The FUSE data were obtained under program P101. FUSE was operated for NASA by the Department of Physics and Astronomy at the Johns Hopkins University. The Green Bank Telescope data were obtained under Program GBT14B-299, and the observatory is a facility of the National Science Foundation, operated under a cooperative agreement by Associated Universities, Inc. D.K. is supported by an NSF Astronomy and Astrophysics Postdoctoral Fellowship under award AST-2102490.

Some of the data presented in this paper were obtained from the Mikulski Archive for Space Telescopes (MAST) at the Space Telescope Science Institute. The specific observations analyzed can be accessed via <https://doi.org/10.17909/t9-axmr-t152>.

Facilities: FUSE, GBT, HST (STIS).

Software: `linetools` (Prochaska et al. 2017), `VPFIT` (Carswell & Webb 2014).

ORCID iDs

Frances H. Cashman  <https://orcid.org/0000-0003-4237-3553>
 Andrew J. Fox  <https://orcid.org/0000-0003-0724-4115>
 Blair D. Savage  <https://orcid.org/0000-0001-8016-6980>
 Bart P. Wakker  <https://orcid.org/0000-0002-0507-7096>
 Dhanesh Krishnarao  <https://orcid.org/0000-0002-7955-7359>
 Robert A. Benjamin  <https://orcid.org/0000-0002-8109-2642>
 Philipp Richter  <https://orcid.org/0000-0002-1188-1435>
 Trisha Ashley  <https://orcid.org/0000-0002-6541-869X>
 Edward B. Jenkins  <https://orcid.org/0000-0003-1892-4423>
 Felix J. Lockman  <https://orcid.org/0000-0002-6050-2008>
 Rongmon Bordoloi  <https://orcid.org/0000-0002-3120-7173>

References

Ackermann, M., Albert, A., Atwood, W. B., et al. 2014, *ApJ*, 793, 64
 Armillotta, L., Fraternali, F., Werk, J. K., Prochaska, J. X., & Marinacci, F. 2017, *MNRAS*, 470, 114

Ashley, T., Fox, A. J., Jenkins, E. B., et al. 2020, *ApJ*, 898, 128
 Bailer-Jones, C. A. L., Rybizki, J., Fousneau, M., Demleitner, M., & Andrae, R. 2021, *AJ*, 161, 147
 Bailly, D., Salumbides, E. J., Vervloet, M., & Ubachs, W. 2010, *MolPh*, 108, 827
 Bland-Hawthorn, J., & Cohen, M. 2003, *ApJ*, 582, 246
 Bland-Hawthorn, J., Maloney, P. R., Sutherland, R., et al. 2019, *ApJ*, 886, 45
 Bordoloi, R., Fox, A. J., Lockman, F. J., et al. 2017, *ApJ*, 834, 191
 Carswell, R. F., & Webb, J. K. 2014, Voigt profile fitting prog ram, Astrophysics Source Code Library, ascl:1408.015
 Di Teodoro, E. M., McClure-Griffiths, N. M., Lockman, F. J., et al. 2018, *ApJ*, 855, 33
 Di Teodoro, E. M., McClure-Griffiths, N. M., Lockman, F. J., & Armillotta, L. 2020, *Natur*, 584, 364
 Dixon, W. V., & Kruk, J. W. 2009, in AIP Conf. Ser. 1135, Future Directions in Ultraviolet Spectroscopy: A Conference Inspired by the Accomplishments of the Far Ultraviolet Spectroscopic Explorer Mission, ed. M. E. van Steenberg et al. (Melville, NY: AIP), 218
 Flower, D. R., & Watt, G. D. 1984, *MNRAS*, 209, 25
 Fox, A. J., Bordoloi, R., Savage, B. D., et al. 2015, *ApJL*, 799, L7
 Fox, A. J., Kumari, N., Ashley, T., Cazzoli, S., & Bordoloi, R. 2021, *RNAAS*, 5, 198
 Ge, J., Bechtold, J., & Black, J. H. 1997, *ApJ*, 474, 67
 Ge, J., Bechtold, J., & Kulkarni, V. P. 2001, *ApJL*, 547, L1
 Gronke, M., & Oh, S. P. 2020, *MNRAS*, 492, 1970
 Heitsch, F., & Putman, M. E. 2009, *ApJ*, 698, 1485
 Jenkins, E. B., & Peimbert, A. 1997, *ApJ*, 477, 265
 Jenkins, E. B., & Tripp, T. M. 2011, *ApJ*, 734, 65
 Jensen, A. G., Snow, T. P., Sonneborn, G., & Rachford, B. L. 2010, *ApJ*, 711, 1236
 Karim, M. T., Fox, A. J., Jenkins, E. B., et al. 2018, *ApJ*, 860, 98
 Keeney, B. A., Danforth, C. W., Stocke, J. T., et al. 2006, *ApJ*, 646, 951
 Krishnarao, D., Benjamin, R. A., & Haffner, L. M. 2020a, *ApJL*, 899, L11
 Krishnarao, D., Benjamin, R. A., & Haffner, L. M. 2020b, *SciA*, 6, 9711
 Liszt, H., & Gerin, M. 2018, *A&A*, 610, A49
 Liszt, H. S., & Burton, W. B. 1980, *ApJ*, 236, 779
 Lockman, F. J., Di Teodoro, E. M., & McClure-Griffiths, N. M. 2020, *ApJ*, 888, 51
 Lockman, F. J., & McClure-Griffiths, N. M. 2016, *ApJ*, 826, 215
 McClure-Griffiths, N. M., Green, J. A., Hill, A. S., et al. 2013, *ApJL*, 770, L4
 Moos, H. W., Cash, W. C., Cowie, L. L., et al. 2000, *ApJL*, 538, L1
 Neufeld, D. A., Melnick, G. J., & Harwit, M. 1998, *ApJL*, 506, L75
 Predehl, P., Sunyaev, R. A., Becker, W., et al. 2020, *Natur*, 588, 227
 Prochaska, J. X., Tejos, N., Crighton, N., et al. 2017, Linetools/Linetools: Third Minor Release, v0.3, Zenodo, doi:10.5281/zenodo.1036773
 Richter, P., de Boer, K. S., Widmann, H., et al. 1999, *Natur*, 402, 386
 Richter, P., Sembach, K. R., Wakker, B. P., & Savage, B. D. 2001, *ApJL*, 562, L181
 Ryans, R. S. I., Dufton, P. L., Keenan, F. P., et al. 1997, *ApJ*, 490, 267
 Savage, B. D., Kim, T.-S., Fox, A. J., et al. 2017, *ApJS*, 232, 25
 Sembach, K. R., Howk, J. C., Savage, B. D., & Shull, J. M. 2001, *AJ*, 121, 992
 Shull, J. M., & Danforth, C. W. 2019, *ApJ*, 882, 180
 Shull, J. M., Danforth, C. W., & Anderson, K. L. 2021, *ApJ*, 911, 55
 Sofue, Y., & Kataoka, J. 2021, *MNRAS*, 506, 2170
 Sparre, M., Pfrommer, C., & Ehlert, K. 2020, *MNRAS*, 499, 4261
 Spitzer, L. J., & Morton, W. A. 1976, *ApJ*, 204, 731
 Su, M., Slatyer, T. R., & Finkbeiner, D. P. 2010, *ApJ*, 724, 1044
 Wakker, B. P. 1991, *A&A*, 250, 499
 Wakker, B. P. 2006, *ApJS*, 163, 282
 Wakker, B. P., Savage, B. D., Sembach, K. R., et al. 2003, *ApJS*, 146, 1
 Zech, W. F., Lehner, N., Howk, J. C., Dixon, W. V. D., & Brown, T. M. 2008, *ApJ*, 679, 460